nature physics

LETTERS

PUBLISHED ONLINE: 4 DECEMBER 2011 | DOI: 10.1038/NPHYS2161

Magnetoelectric resonance with electromagnons in a perovskite helimagnet

Youtarou Takahashi[1]*, Ryo Shimano[1,2], Yoshio Kaneko[1], Hiroshi Murakawa[1] and Yoshinori Tokura[1,3,4]

Maxwell's equations describe the interrelation between temporally changing electric (*E*) and magnetic (*H*) fields in a given medium. In materials that exhibit relativistic spin–orbit interactions, we also expect their polarization (*P*) and magnetization (*M*) to be dynamically coupled. This in turn could enable greater control over the cross-coupling between the electric and magnetic fields of light in the development of photonic devices[1]. Such magnetoelectric phenomena are expected to be enhanced within materials that support electromagnons—fundamental excitations that exhibit both electric and magnetic dipole moments. Here we report the discovery of electromagnons in the perovskite (Eu, Y)MnO_3, which arise from fluctuations in the spontaneous polarization generated by cycloidal spin order[2–5]. The resulting dynamical *M*–*P* cross-coupling causes the material to exhibit colossal directional dichroism—a difference in the absorption of light propagating in opposite directions—at the resonance frequency (sub-THz) associated with these excitations.

The magnetoelectric effect, which is the cross-correlation between electricity and magnetism, is one of the central subjects in contemporary condensed-matter science. Although the magnetoelectric effect itself has a long history of investigations[6], the recent discovery of the large magnetoelectric effect in multiferroics, in which particular spin orders produce ferroelectric polarization, accelerates the research of this area[2,3,7]. Among them, a unique origin of ferroelectricity has been found in perovskite $RMnO_3$ (R = rare earth), where the helical spin structure produces the macroscopic electric polarization irrespective of the original lattice symmetry. The origin of this ferroelectricity is successfully explained by the spin-current model, or equivalently the inverse effect of the Dzyaloshinskii–Moriya interaction[4,8]; the microscopic polarization around the bond connecting adjacent spins is produced by the term proportional to vector product $\mathbf{e}_{ij} \times (\mathbf{S}_i \times \mathbf{S}_j)$, where $\mathbf{e}_{ij}$ is a unit vector connecting the adjacent spins $\mathbf{S}_i$ and $\mathbf{S}_j$. In this model, the spontaneous spin current is viewed as flowing between the mutually canted spins ($\mathbf{S}_i$ and $\mathbf{S}_j$) with the magnetization component along the direction of $(\mathbf{S}_i \times \mathbf{S}_j)$, which in turn generates the electronic polarization under the spin–orbit interaction. The summation of these microscopic polarizations gives rise to the ferroelectricity in the cycloidal (transverse-spiral) spin structure, where the static polarization lies in the helical spin plane and is directed perpendicular to the magnetic modulation vector $\mathbf{q}_m$ (Fig. 1a).

Such magnetically driven ferroelectricity promises a concomitant collective spin excitation endowed with electric dipole activity, termed an electromagnon[9]. In the cycloidal spin phase, the rotational vibration of the helical spin plane accompanies that of the ferroelectric polarization (mode I in Fig. 1b), leading to the electric activity of this magnetic excitation as the electromagnon[5]. However, the existence of this magnetic excitation generic for multiferroic order has remained controversial[9–14]; spin excitations with transition electric dipoles have in fact been observed for several multiferroics, but their origins have now been identified to be different from the above cross-coupling electromagnon; that mode is induced by the magnetostriction mechanism, unrelated to spin–orbit interaction, and shows no magnetic-dipole activity[15–19]. In this study, we have unravelled the cross-coupling electromagnon driven by the spin-current mechanism in a perovskite manganite $Eu_{0.55}Y_{0.45}MnO_3$ as well as its generic dynamical magnetoelectric effect.

In $Eu_{0.55}Y_{0.45}MnO_3$, the spin structure exhibits the *ab*-plane cycloidal spin phase in the ground state with $\mathbf{q}_m \parallel b$ axis (Fig. 1a)[20]. With the onset of the *ab*-plane cycloidal spin phase, the ferroelectric polarization directed along the *a* axis shows up as predicted by the spin-current model. In the terahertz regime, a strongly electric-dipole-active absorption is observed when the light electric vector $\mathbf{E}^{\omega}$ is parallel to the *a* axis as shown in Fig. 1c. This $\mathbf{E}^{\omega} \parallel a$ electromagnon is commonly observed in the helical spin phase in $RMnO_3$ compounds irrespective of the spin-spiral plane configuration (*ab* or *bc* plane), and has been elucidated in terms of the magnetostriction mechanism; the electric field of light acts on the local electric dipole produced by $GaFeO_3$-type lattice distortion, which in turn modulates the exchange interaction between the adjacent spins and gives rise to the in-plane spin rotational vibration (mode III shown in Fig. 1b)[18,19]. Although the electromagnon arising from this magnetostriction mechanism corresponds to the zone-edge magnon mode ($q = \pi$; refs 18,19; 8 meV for this material[21]), it has been shown[22] that magnetic anisotropy terms induce the low-energy peak of the electromagnon with $q = \pi - 2q_m$ at 2.4 meV, as plotted in Fig. 1c. Note that such a magnetostriction-induced electromagnon mode with the electric-dipole activity is, however, not magnetic-dipole active owing to their $q \neq 0$ and $q \neq q_m$ nature, lacking in cross-coupling nature (see Supplementary Information).

The electromagnon of spin-current origin, on the other hand, should be active for $\mathbf{E}^{\omega} \parallel c$ polarization in the case of *ab*-plane cycloidal spin structure where the static ferroelectric polarization $\mathbf{P}$ is directed along the *a* axis (mode I shown in Fig. 1b). Figure 1d,e shows the spectra of the imaginary parts of the refractive indices under the external magnetic field along the *c* axis. A distinct

[1]Multiferroics Project, ERATO, Japan Science and Technology Agency (JST), Tokyo 113-8656, Japan, [2]Department of Physics, The University of Tokyo, Tokyo 113-0033, Japan, [3]Department of Applied Physics and Quantum Phase Electronics Center (QPEC), University of Tokyo, Tokyo 113-8656, Japan, [4]Cross-Correlated Materials Research Group (CMRG) and Correlated Electron Research Group (CERG), RIKEN Advanced Science Institute, Wako 351-0198, Japan. *e-mail: youtarou-takahashi@ap.t.u-tokyo.ac.jp.

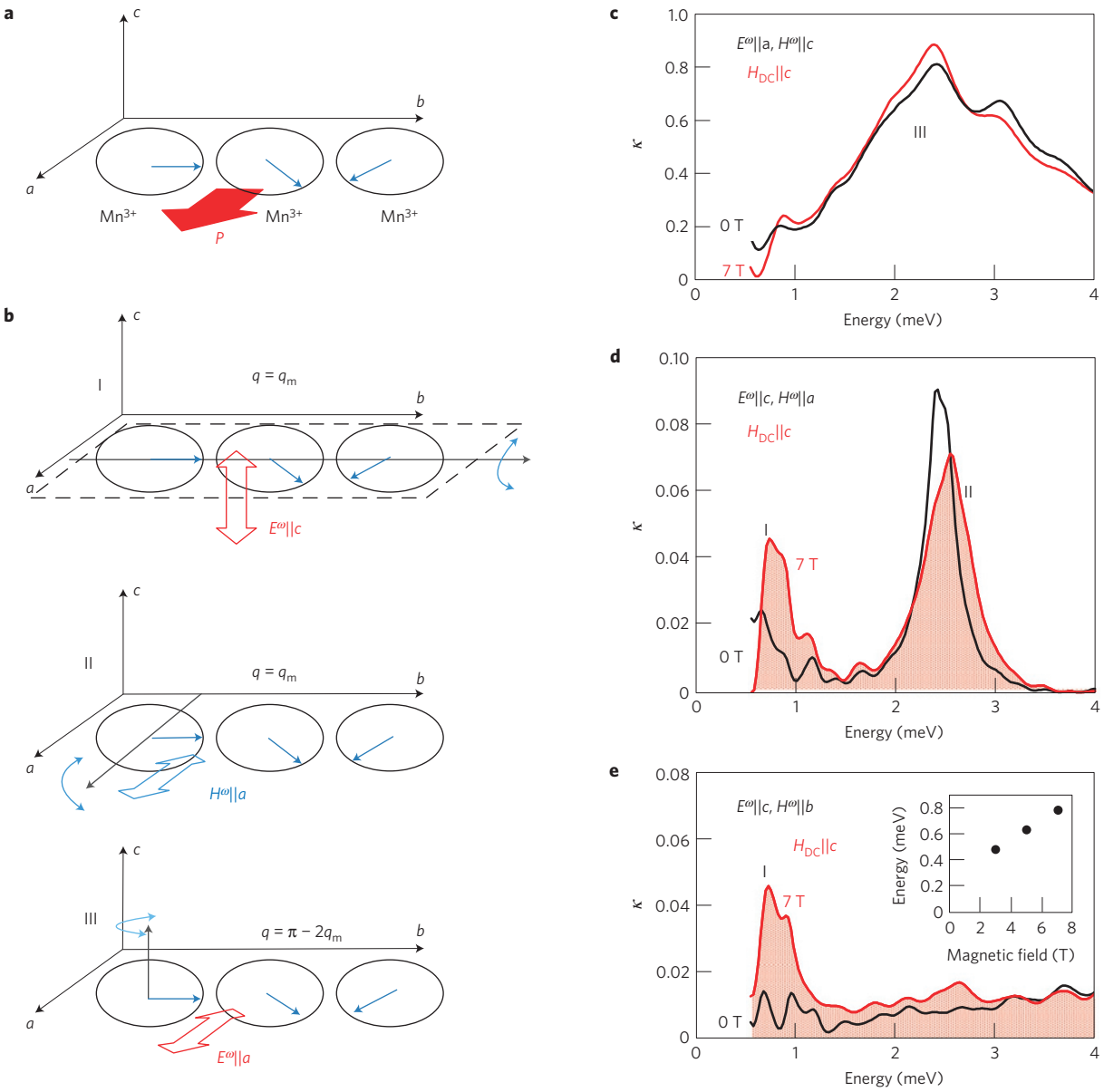

Figure 1 | Spin excitations in cycloidal spin state. a, Schematic spin structure and direction of static ferroelectric polarization in the *ab*-plane cycloidal spin phase. **b**, Illustration of the spin motion. Mode I (cross-coupling electromagnon): rotational vibration of the helical spin plane around the *b* axis. Mode II (magnon): rotational vibration of the spins around the *a* axis. Mode III (magnetostriction-induced electromagnon): rotational vibration of the spins around the *c* axis. Wavenumbers of the magnons are also indicated. **c**–**e**, Imaginary part κ of the refractive index for ($\mathbf{E}^{\omega} \parallel a$, $\mathbf{H}^{\omega} \parallel c$) (**c**), ($\mathbf{E}^{\omega} \parallel c$, $\mathbf{H}^{\omega} \parallel a$) (**d**) and ($\mathbf{E}^{\omega} \parallel c$, $\mathbf{H}^{\omega} \parallel b$) (**e**) under the external magnetic field along the *c* axis at 4 K. The inset in **e** shows the magnetic-field dependence of the energy of mode I. (Tiny structures in κ around 1 meV at 0 T are background or artefact, showing little temperature dependence.)

peak structure appears at 0.8 meV (7 T) for both ($\mathbf{E}^{\omega} \parallel c$, $\mathbf{H}^{\omega} \parallel a$) (Fig. 1d) and ($\mathbf{E}^{\omega} \parallel c$, $\mathbf{H}^{\omega} \parallel b$) (Fig. 1e), signalling the electric activity of this mode. (Note that mode I is also active for $\mathbf{H}^{\omega} \parallel b$, and hence spectra in Fig. 1e may contain some amount of magnetically active component.) This makes a strong contrast with the peak structure at 2.7 meV in Fig. 1d, which is absent from Fig. 1e and has been attributed to the conventional antiferromagnetic resonance (AFMR) driven by the $\mathbf{H}^{\omega} \parallel a$ component of light (mode II in Fig. 1b). The electromagnon observed at about 0.8 meV can be identified as the Nambu–Goldstone mode of the cycloidal spin order[5,13]; the magnetic anisotropy due to the energy difference between the *ab*- and *bc*-plane helical states as well as to the external magnetic field induces the finite resonance energy as observed. The resonance energy increases with the magnetic field (inset to Fig. 1e), because the magnetic field along the *c* axis stabilizes the *ab*-plane helical state[20], leading to an increase of the magnetic anisotropy.

The energies of magnons including electromagnons observed by the terahertz spectroscopy are compatible with the result of polarized inelastic neutron scattering experiments on $TbMnO_3$ (refs 10,11), of which the magnon dispersion is plausibly similar to that of $Eu_{0.55}Y_{0.45}MnO_3$. The magnons in the *bc*-plane cycloidal spin state of $TbMnO_3$ exhibit three branches at (0, q_m, 1). Two modes with out-of-plane dynamical spin component at about 1.1 and 2.5 meV can be ascribed to the spin-current-driven electromagnon (mode I) and AFMR (mode II), respectively, whereas the electromagnon due to magnetostriction (mode III) is attributed to the magnon at another *k* point.

One of the most intriguing aspects of this spin-current-driven electromagnon is its dynamical magnetoelectric effect,

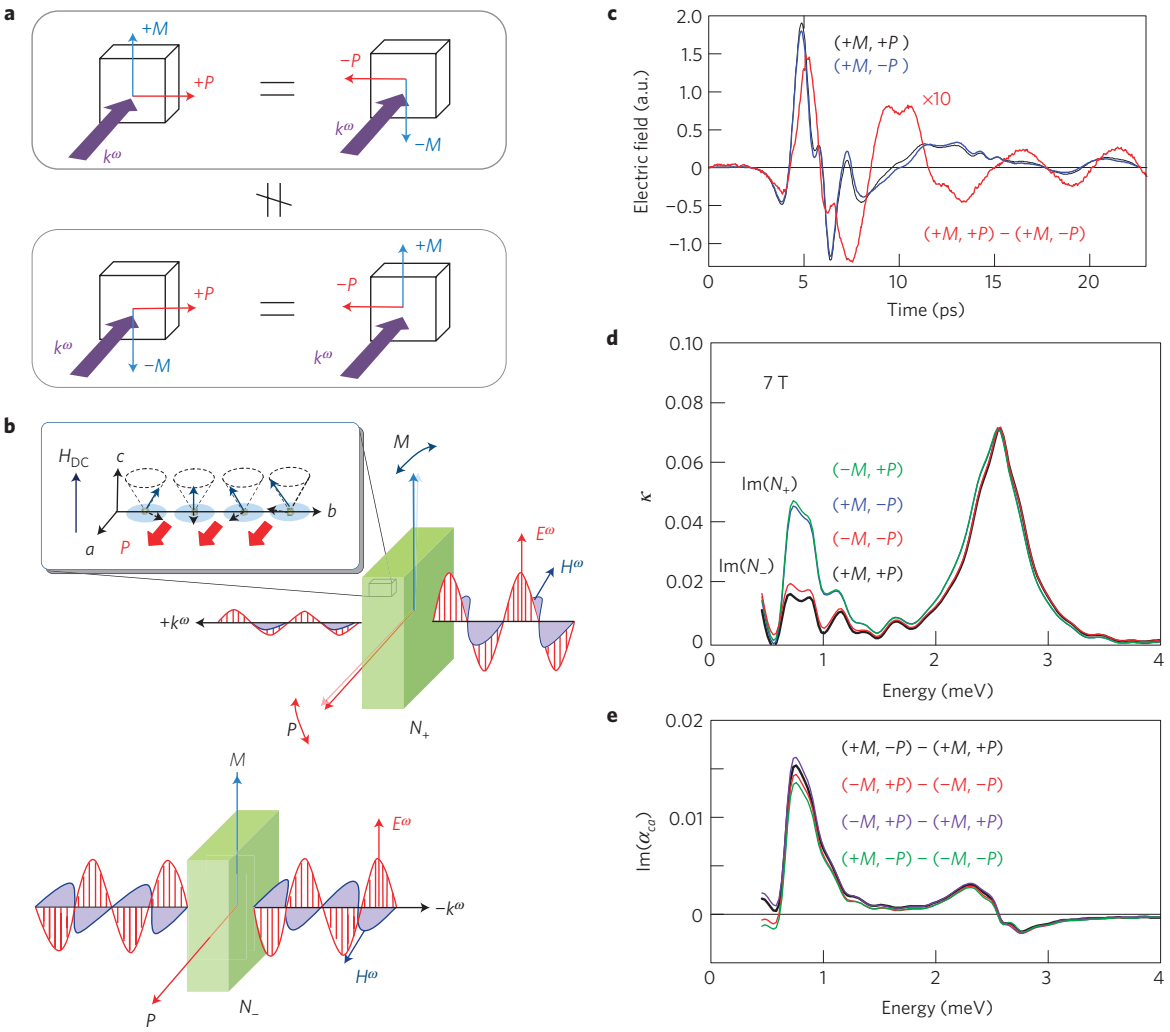

Figure 2 | Experimental observation of magnetoelectric resonance. a, Configurations of **P**, **M** and $\mathbf{k}^{\omega}$ and their relation in terms of the optical magnetoelectric effect (see text). **b**, Experimental configuration for the matter (**P** and **M**), and for the light ($\mathbf{E}^{\omega}$, $\mathbf{H}^{\omega}$ and $\mathbf{k}^{\omega}$) with respect to two different conditions of $\pm k^{\omega}$ ($N_{\pm}$). $\mathbf{E}^{\omega}$ and $\mathbf{H}^{\omega}$ of light with $+\mathbf{k}^{\omega}$ can constructively vibrate both **P** and **M** (upper panel), whereas $\mathbf{E}^{\omega}$ and $\mathbf{H}^{\omega}$ of $-\mathbf{k}^{\omega}$ suppress the vibrations of **P** and **M** with each other (lower panel). **c**, Time-domain waveform of the transmitted terahertz pulses in different configurations in terms of the magnetoelectric effect (black and blue lines) and the difference between them (red line) at 7 T. **d**, Imaginary part of refractive index for $\mathbf{E}^{\omega} \parallel c$, $\mathbf{H}^{\omega} \parallel a$ under magnetic field along the *c* axis (7 T) at 4 K. Spectra for the four possible configurations in **a** are shown. **e**, Imaginary part of α_{ca}. Results for four possible combinations to obtain $\mathrm{Im}(\alpha_{ca})$ are shown.

arising from the strong cross-coupling between the induced polarization $\mathbf{P}^{\omega}$ and magnetization $\mathbf{M}^{\omega}$. The dynamical response of the first-order magnetoelectric coupling can be described by the dynamical magnetoelectric tensor $\alpha_{ij}(\omega)$ in addition to the conventional terms (dynamical dielectric and magnetic susceptibility) $\chi^{\mathrm{ee}}(\omega)$ and $\chi^{\mathrm{mm}}(\omega)$,

$$\begin{aligned} P_i^{\omega} &= \chi_{ii}^{\mathrm{ee}}(\omega)E_i^{\omega} + \alpha_{ij}(\omega)H_j^{\omega} \\ M_j^{\omega} &= \chi_{jj}^{\mathrm{mm}}(\omega)H_j^{\omega} + \alpha_{ij}(\omega)E_i^{\omega} \end{aligned} \qquad (1)$$

To enable the existence of the magnetoelectric tensor, the symmetry consideration requires the simultaneous breaking of time-reversal and space-inversion symmetry, for example the configuration shown in Fig. 2a with the orthogonal relations among **P**, **M** and light wavevector $\mathbf{k}^{\omega}$ (ref. 23). (Note that **P** and **M** are the static quantities here.) When this condition is satisfied, the optical magnetoelectric effect for the linearly polarized light can appear with directional non-reciprocity; light with $\mathbf{k}^{\omega}$ vectors parallel and antiparallel to $\mathbf{P} \times \mathbf{M}$ experiences different optical responses (Fig. 2b). By combining Maxwell's equations with equation (1), the directional complex refractive index is given for $\pm\mathbf{k}^{\omega}$:

$$N_{\pm}(\omega) = n(\omega) + i\kappa(\omega) = (n_0(\omega) + i\kappa_0(\omega)) \pm \alpha_{ij}(\omega) \qquad (2)$$

where n_0 and κ_0 are the conventional (non-magnetoelectric) parts of the refractive index[24]. The real and imaginary parts of $\alpha_{ij}(\omega)$ contribute to the directional birefringence and dichroism, respectively. The reversal of one of three parameters (**P**, **M** and $\mathbf{k}^{\omega}$) results in a sign change of $\alpha_{ij}(\omega)$ in the refractive index $N_{\pm}(\omega)$. To observe the non-reciprocal dichroism, we carried out the experiments in four configurations of ($\mathbf{k}^{\omega}$, **P**, **M**), which are categorized into two equivalent configurations in terms of the sign of the product, $\mathbf{k}^{\omega} \cdot (\mathbf{P} \times \mathbf{M})$ (see Fig. 2a). As no spontaneous magnetization appears in the cycloidal spin state, we applied an external magnetic field along the *c* axis to induce the cone-like transverse helical spin structure and therefore cause a finite static magnetization **M** along the *c* axis. As a result, the coexistence of spontaneous ferroelectric polarization $\mathbf{P} \parallel a$ and field-induced magnetization $\mathbf{M} \parallel c$ gives rise to a finite

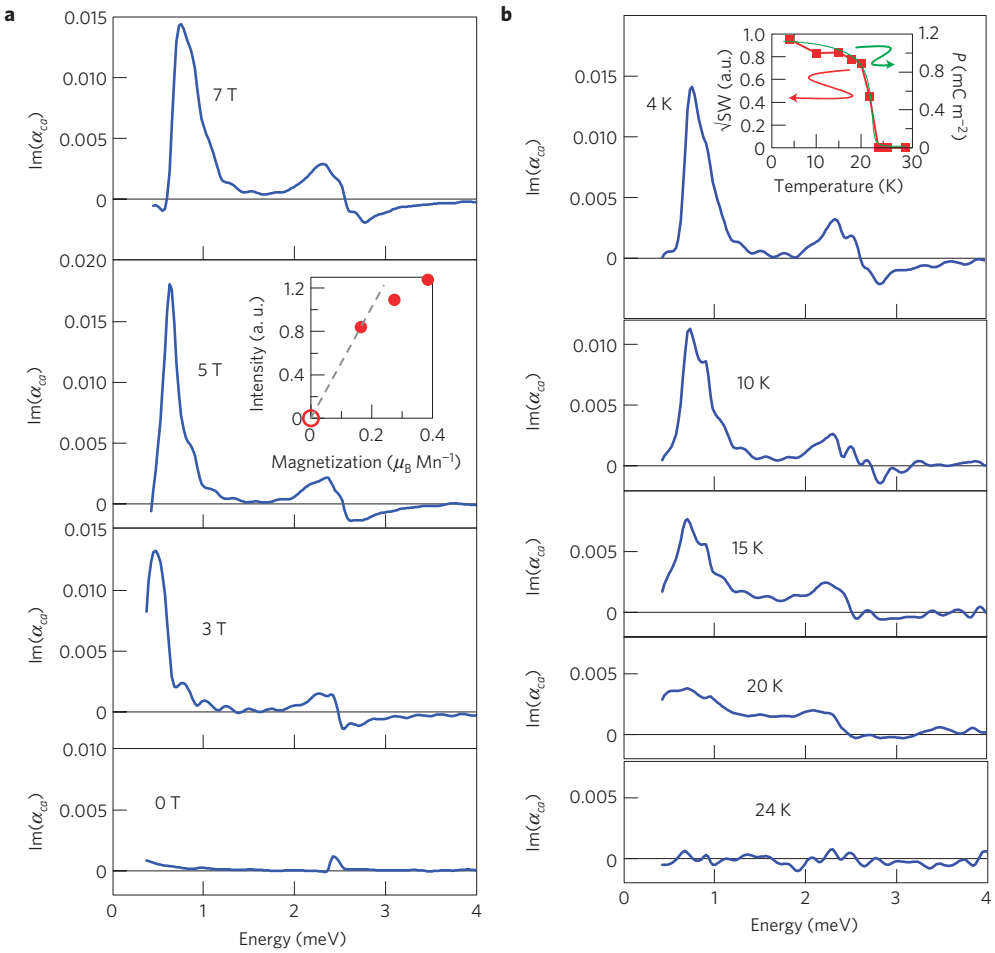

Figure 3 | Temperature and magnetic-field dependence of magnetoelectric resonance spectra. a,Magnetic-field dependence of Im(α_{ca}) at 4 K. Inset: The magnetization dependence of the integrated intensity of Im(α_{ca}) at the electromagnon resonance (red filled circles), which shows the deviation from the linear magnetic-field dependence (grey dashed line). No magnetoelectric effect is anticipated in zero magnetic field (as indicated with a red open circle), because the time-reversal invariance of the cycloid spin state prohibits the magnetoelectric effect. **b**, Temperature dependence of Im(α_{ca}) at 7 T. Inset: The temperature dependence of spontaneous polarization and square root of spectral weight (SW) of Im(α_{ca}).

value of $\mathbf{P}\times\mathbf{M}(\|\mathbf{b})$; the light polarization of ($\mathbf{E}^{\omega}\|c$, $\mathbf{H}^{\omega}\|a$) is selected to enable both magnetic and electric resonances with the spin-current-driven electromagnon with the light $\mathbf{k}^{\omega}$-vector along the *b* axis.

As shown in Fig. 2c, the temporal waveform of the terahertz pulse transmitted through the sample shows a distinct difference depending on the sign of $\mathbf{P}\times\mathbf{M}$, indicating the occurrence of the dynamical magnetoelectric effect. The subtracted waveform exhibits a low-frequency oscillation with a period of 5.2 ps, which corresponds to 0.8 meV in photon energy. In fact, the imaginary part of the refractive index κ shows a dramatic difference between the two inequivalent configurations at the electromagnon resonance, in contrast to the AFMR at 2.7 meV, which mostly conserves its intensity (Fig. 2d). The spectra of the 0.8 meV resonance exhibit the enhanced absorption (Im(N_+)) with $\mathbf{k}^{\omega}$ parallel to $\mathbf{P}\times\mathbf{M}$, but the suppressed one (Im(N_-)) for $\mathbf{k}^{\omega}$ antiparallel to $\mathbf{P}\times\mathbf{M}$. This difference directly gives the component of the magnetoelectric tensor α_{ca} for light polarization of ($\mathbf{E}^{\omega}\|c$, $\mathbf{H}^{\omega}\|a$); Im(α_{ca}) = (Im(N_+) − Im(N_-))/2 (see equation (2)). As shown in Fig. 2e, a colossal directional dichroism is discerned at the resonance of the spin-current-driven electromagnon even for small $\mathbf{M}$ (0.37 μ_B/Mn^{3+} at 7 T), which is less than 10% of the fully spin-polarized value (4 μ_B/Mn^{3+}). Although the maximum value of Im(α_{ca}) is restricted by the second law of thermodynamics as given by $\kappa = \kappa_0 - \mathrm{Im}(\alpha_{ca}) > 0$, the observed magnitude of Im(α_{ca}) (∼0.15) approaches roughly 50% of κ_0 (=($\kappa_+ + \kappa_-$)/2 ∼ 0.03) at 7 T, namely the same order as κ_0. The first observation of the optical magnetoelectric effect has been reported on the electronic transition on the isolated rare-earth ions in garnet with relatively small magnitude (∼10^{-3}%; ref. 23). Recently, enhancement of the magnetoelectric effect has been reported on several particular electronic and magnetic resonances, which are the transitions of the local *d* electron in the ligand field in X-ray[25], visible and near-infrared[26,27] and far-infrared regions[28]. In the present case, the colossal dynamical magnetoelectric effect emerges at the resonance of the spin-current-driven electromagnon with both electric- and magnetic-dipole activities as the dynamical counterpart of the large static magnetoelectric effect in the multiferroic system. Incidentally, this kind of dynamical magnetoelectric effect can be distinguished from the other type of magnetoelectric coupling on magnetostrictive–piezoelectric devices, where the magnetic resonance is coupled with the static electric field through strain[6,29]. On the other hand, the magnetoelectric resonance observed at present may be viewed as the dynamical resonance of toroidal moment[30], as the static toroidal (ferrotoroidic) moment is always anticipated under the existence of $\mathbf{P}\times\mathbf{M}$.

A relatively small but finite magnetoelectric effect appears around 2.5 meV as shown in Fig. 2e, indicating that the originally genuine AFMR (mode II) gains magnetoelectric coupling in the magnetic field. Although the AFMR shows basically no electric

activity, this result suggests that the finite electric activity shows up in the **H**-induced conical spin state. In fact, the electric component of AFMR for $\mathbf{E}^{\omega} \parallel c$ is manifested by the tiny structures around 2.6 meV at 7 T as shown in Fig. 1e. The electric activity of AFMR may be induced by the transfer of the spectral weight from the electromagnons through the H-induced coupling among these excitations.

Figure 3a shows the magnetic-field dependence of $\mathrm{Im}(\alpha_{ca})$, which is relevant to the sign and magnitude of $\mathbf{P} \times \mathbf{M}$. In the present condition, **P** is nearly constant and **M** is proportional to the magnetic field. Near $H = 0$, $\mathrm{Im}(\alpha_{ca})$ should be proportional to **M**, because $\mathrm{Im}(\alpha_{ca})$ originates from the first-order magnetoelectric effect with respect to **M** and **P**. Indeed, $\mathrm{Im}(\alpha_{ca})$ increases with magnetic field (Fig. 3a); however, a deviation from linear **M** dependence is observed (inset to Fig. 3a), indicating that the $\mathrm{Im}(\alpha_{ca})$ goes beyond the linear regime to **M**.

Figure 3b shows the temperature dependence of the dynamical magnetoelectric effect. Apparently, the magnetoelectric effect emerges below 23 K (ref. 20), where the helical spin state appears. The temperature dependence of the spectral weight of $\mathrm{Im}(\alpha_{ca})$ is plotted in the inset of Fig. 3b, showing a good agreement with the temperature dependence of $\mathbf{P}^2$. Because this electromagnon has its origin in the fluctuation of the spontaneous **P**, this coincidence confirms the assignment of this electromagnon to the rotational vibration mode of the helical spin plane (Fig. 1bI).

A magnetoelectric resonance originating from the fluctuation in **P** as observed in the present study should be ubiquitous for any magnetically driven ferroelectrics (for example multiferroic helimagnets), and is always expected to give rise to the dynamical magnetoelectric effect in a gigahertz-to-terahertz frequency region. The extension of the magnetoelectric effect toward the dynamical region may open a new arena in the control of electromagnetism of materials beyond the conventional optics.

Methods

Single crystals of orthorhombic perovskite $Eu_{0.55}Y_{0.45}MnO_3$ were grown by the floating-zone method. To obtain the value of ferroelectric polarization, pyroelectric current was measured after cooling with the electric field of $\pm 400\ \mathrm{V\,cm^{-1}}$ along the *a* axis and the magnetic field of 7 T along the *c* axis. Terahertz time-domain spectroscopy was carried out under the magnetic field applied perpendicular to the light propagation direction (in the Voigt configuration) to determine the complex refractive index in the energy range from 0.4 to 4 meV. A femtosecond laser pulse was split into two paths to generate and detect the terahertz wave. The terahertz pulse was emitted from a bow-tie-shape photoconductive antenna and detected by a dipole antenna. To observe the dynamical magnetoelectric effect due to the spin-current-driven electromagnon, the polarization configuration of ($\mathbf{E}^{\omega} \parallel c$, $\mathbf{H}^{\omega} \parallel a$) was employed (Fig. 2b). The sample was placed in a superconducting magnet, which can apply magnetic field up to 7 T. To measure the optical magnetoelectric effect, d.c. electric field of $1\ \mathrm{kV\,cm^{-1}}$ was applied to the sample during the cooling process and then switched off at 4 K, so that a single ferroelectric domain was formed. During the terahertz measurements, no d.c. electric field was applied to the sample.

Received 14 July 2011; accepted 3 November 2011; published online 4 December 2011

References

1. Barron, L. D. *Molecular Light Scattering and Optical Activity* (Cambridge Univ. Press, 2004).
2. Cheong, S-W. & Mostovoy, M. Multiferroics: A magnetic twist for ferroelectricity. *Nature Mater.* **6,** 13–20 (2007).
3. Tokura, Y. & Seki, S. Multiferroics with spiral spin orders. *Adv. Mater.* **22,** 1554–1565 (2010).
4. Katsura, H., Nagaosa, N. & Balatsky, A. V. Spin current and magnetoelectric effect in noncollinear magnets. *Phys. Rev. Lett.* **95,** 057205 (2005).
5. Katsura, H., Balatsky, A. V. & Nagaosa, N. Dynamical magnetoelectric coupling in helical magnets. *Phys. Rev. Lett.* **98,** 027203 (2007).
6. Eerenstein, W., Mathur, N. D. & Scott, J. F. Multiferroic and magnetoelectric materials. *Nature* **442,** 759–765 (2006).
7. Kimura, T. *et al.* Magnetic control of ferroelectric polarization. *Nature* **426,** 55–58 (2003).
8. Mostovoy, M. Ferroelectricity in spiral magnets. *Phys. Rev. Lett.* **96,** 067601 (2006).
9. Pimenov, A. *et al.* Possible evidence for electromagnons in multiferroic manganites. *Nature Phys.* **2,** 97–100 (2006).
10. Senff, D. *et al.* Magnetic excitations in multiferroic $TbMnO_3$: Evidence for a hybridized soft mode. *Phys. Rev. Lett.* **98,** 137206 (2007).
11. Senff, D. *et al.* Magnetic excitations in a cycloidal magnet: The magnon spectrum of multiferroic $TbMnO_3$. *J. Phys. Condens. Matter* **20,** 434212 (2008).
12. Shuvaev, A. M. *et al.* Evidence for electroactive excitation of the spin cycloid in $TbMnO_3$. *Phys. Rev. Lett.* **104,** 097202 (2010).
13. Furukawa, S., Sato, M. & Onoda, S. Chiral order and electromagnetic dynamics in one-dimensional multiferroic cuprates. *Phys. Rev. Lett.* **105,** 257205 (2010).
14. Hüvonen, D. *et al.* Magnetic excitations and optical transitions in the multiferroic spin-1/2 system $LiCu_2O_2$. *Phys. Rev. B* **80,** 100402(R) (2009).
15. Sushkov, A. B. *et al.* Electromagnons in multiferroic YMn_2O_5 and $TbMn_2O_5$. *Phys. Rev. Lett.* **98,** 027202 (2007).
16. Kida, N. *et al.* Electric-dipole-active magnetic resonance in the conical-spin magnet $Ba_2Mg_2Fe_{12}O_{22}$. *Phys. Rev. B* **80,** 220406(R) (2009).
17. Takahashi, Y. *et al.* Electromagnons in the multiferroic state of perovskite manganites with symmetric exchange striction. *Phys. Rev. B* **81,** 100413(R) (2010).
18. Valdés Aguilar, R. *et al.* Origin of electromagnon excitations in multiferroic $RMnO_3$. *Phys. Rev. Lett.* **102,** 047203 (2009).
19. Lee, J. S. *et al.* Systematics of electromagnons in the spiral spin-ordered states of $RMnO_3$. *Phys. Rev. B* **79,** 180403(R) (2009).
20. Murakawa, H. *et al.* Rotation of an electric polarization vector by rotating magnetic field in cycloidal magnet $Eu_{0.55}Y_{0.45}MnO_3$. *Phys. Rev. Lett.* **101,** 197207 (2008).
21. Takahashi, Y. *et al.* Far-infrared optical study of electromagnons and their coupling to optical phonons in $Eu_{1-x}Y_xMnO_3$ ($x = 0.1$, 0.2, 0.3, 0.4, and 0.45). *Phys. Rev. B* **79,** 214431 (2009).
22. Mochizuki, M., Furukawa, N. & Nagaosa, N. Theory of electromagnons in the multiferroic Mn perovskites: The vital role of higher harmonic components of the spiral spin order. *Phys. Rev. Lett.* **104,** 177206 (2010).
23. Rikken, G. L. J. A., Strohm, C. & Wyder, P. Observation of magnetoelectric directional anisotropy. *Phys. Rev. Lett.* **89,** 133005 (2002).
24. Hornreich, R. M. & Shtrikman, S. Theory of gyrotropic birefringence. *Phys. Rev.* **171,** 1065–1074 (1968).
25. Kubota, M. *et al.* X-ray directional dichroism of a polar ferrimagnet. *Phys. Rev. Lett.* **92,** 137401 (2004).
26. Jung, J. H. *et al.* Optical magnetoelectric effect in the polar $GaFeO_3$ ferrimagnet. *Phys. Rev. Lett.* **93,** 037403 (2004).
27. Saito, M., Taniguchi, K. & Arima, T. Gigantic optical magnetoelectric effect in CuB_2O_4. *J. Phys. Soc. Jpn* **77,** 013705 (2008).
28. Kézsmárki, I. *et al.* Enhanced directional dichroism of terahertz light in resonance with magnetic excitations of the multiferroic $Ba_2CoGe_2O_7$ oxide compound. *Phys. Rev. Lett.* **106,** 057403 (2011).
29. Nan, C-W. *et al.* Multiferroic magnetoelectric composites: Historical perspective, status, and future directions. *J. Appl. Phys.* **103,** 031101 (2008).
30. Spaldin, N. A., Fiebig, M. & Mostovoy, M. The toroidal moment in condensed-matter physics and its relation to the magnetoelectric effect. *J. Phys. Condens. Matter* **20,** 434203 (2008).

Acknowledgements

The authors thank N. Nagaosa, T. Arima, N. Furukawa and S. Miyahara for fruitful discussion. This research was supported in part by the Japan Society for the Promotion of Science (JSPS) through the 'Funding Program for World-Leading Innovative R&D on Science and Technology (FIRST Program)', initiated by the Council for Science and Technology Policy (CSTP).

Author contributions

Y. Takahashi carried out optical terahertz spectroscopy and analysed data. Y.K. carried out crystal growth. H.M. measured pyroelectric current. The results were discussed and interpreted by Y. Takahashi, R.S. and Y. Tokura.

Additional information

The authors declare no competing financial interests. Supplementary information accompanies this paper on www.nature.com/naturephysics. Reprints and permissions information is available online at http://www.nature.com/reprints. Correspondence and requests for materials should be addressed to Y. Takahashi.